

Anomalous Fermi surface in FeSe seen by Shubnikov-de Haas oscillation measurements

Taichi Terashima,¹ Naoki Kikugawa,¹ Andhika Kiswandhi,² Eun-Sang Choi,² James S. Brooks,² Shigeru Kasahara,³ Tatsuya Watashige,³ Hiroaki Ikeda,^{3,4} Takasada Shibauchi,^{3,5} Yuji Matsuda,³ Thomas Wolf,⁶ Anna E. Böhrer,⁶ Frédéric Hardy,⁶ Christoph Meingast,⁶ Hilbert v. Löhneysen,⁶ Michi-To Suzuki,⁷ Ryotaro Arita,⁷ and Shinya Uji¹

¹*National Institute for Materials Science, Tsukuba, Ibaraki 305-0003, Japan*

²*National High Magnetic Field Laboratory, Florida State University, Tallahassee, FL 32310, USA*

³*Department of Physics, Kyoto University, Kyoto 606-8502, Japan*

⁴*Department of Physical Sciences, Ritsumeikan University, Kusatsu, Shiga 525-8577, Japan*

⁵*Department of Advanced Materials Science, University of Tokyo, Chiba 277-8561, Japan*

⁶*Institute of Solid State Physics (IFP), Karlsruhe Institute of Technology, D-76021 Karlsruhe, Germany*

⁷*RIKEN Centre for Emergent Matter Science, Wako 351-0198, Japan*

(Dated: March 2, 2022)

We have observed Shubnikov-de Haas oscillations in FeSe. The Fermi surface deviates significantly from predictions of band-structure calculations and most likely consists of one electron and one hole thin cylinder. The carrier density is in the order of 0.01 carriers/Fe, an order-of-magnitude smaller than predicted. Effective Fermi energies as small as 3.6 meV are estimated. These findings call for elaborate theoretical investigations incorporating both electronic correlations and orbital ordering.

PACS numbers: 74.70.Xa, 71.18.+y, 74.25.Jb, 74.25.Op

I. INTRODUCTION

FeSe is an intriguing material among iron-based superconductors: The FeSe planes are isoelectronic with the (FeAs)⁻¹ planes of the archetypal parent compounds of iron-based superconductors such as LaFeAsO (Ref. 1) or BaFe₂As₂.² However, FeSe shows only a structural phase transition at $T_s \sim 100$ K without an accompanying magnetic phase transition and becomes superconducting below $T_c \sim 8$ K.³ For comparison, BaFe₂As₂ has structural and antiferromagnetic phase transitions at 140 K but does not exhibit superconductivity.² As both transitions are suppressed by partial substitution of Ba, Fe, or As atoms, superconductivity emerges.^{2,4} Although the nature of the transition at T_s in FeSe is not yet clear, angle-resolved photoemission spectroscopy (ARPES) measurements on FeSe have found a splitting of the d_{xz} and d_{yz} bands at the corner of the Brillouin zone below ~ 110 K,⁵⁻⁷ similar to one found in BaFe₂As₂,⁸ suggesting orbital order.⁹ Secondly, the onset temperature of superconductivity can be enhanced up to ~ 37 K by application of pressure.^{10,11} Moreover, it has recently been claimed that T_c in single-layer FeSe films may exceed 50 K.¹² Finally, very recent magnetotransport, penetration depth, and spectroscopic-imaging scanning tunneling microscopy (STM) measurements on vapor-grown high-quality FeSe single crystals suggest that the Fermi energy E_F is extremely small and comparable to the superconducting energy gap Δ ,¹³ as observed previously in Te-substituted alloys Fe(Se, Te) by ARPES measurements.^{14,15} FeSe may therefore be in the Bardeen-Cooper-Schrieffer (BCS)–Bose-Einstein-condensation (BEC) crossover regime.

Detailed research into the *bulk* electronic structure of FeSe is necessary to advance our understanding of

these intriguing properties of FeSe, but such research was impeded by difficulties in single-crystal growth. Recently, Böhrer *et al.*¹⁶ have grown FeSe single crystals of unprecedented quality using a vapor transport technique. X-ray structural refinement has indicated a composition of Fe_{0.995(4)}Se.¹⁶ The composition very close to stoichiometry has further been confirmed by STM topographs as well as magnetotransport data indicating a nearly perfect carrier compensation.¹³ Using those crystals, we were able to observe Shubnikov-de Haas (SdH) oscillations in FeSe. Our central finding is that the observed Fermi surface (FS) is extremely small and strikingly different from band-structure calculations.

II. EXPERIMENTS

Standard four-contact resistance (R) measurements were performed with a 35-T resistive magnet and ³He or ³He/⁴He dilution refrigerator at the NHMFL. The electrical contacts were spot-welded. The magnetic field (B) direction θ is measured from the crystallographic c axis. Four samples with T_c and the resistance ratio (between room temperature and 11 K) of 8.9–9.2 K and 28–32, respectively, were investigated, and consistent results were obtained.

For a purely two-dimensional FS cylinder, there would be a single SdH frequency F , and $F \cos \theta$ would remain constant as θ is varied. However, in real materials, there is some c -axis dispersion, which modulates the cross-section of the FS cylinder. In simple cases, two frequencies corresponding to the minimum and maximum cross-sections will appear and will exhibit upward and downward variations of $F \cos \theta$, respectively, as $|\theta|$ is increased.

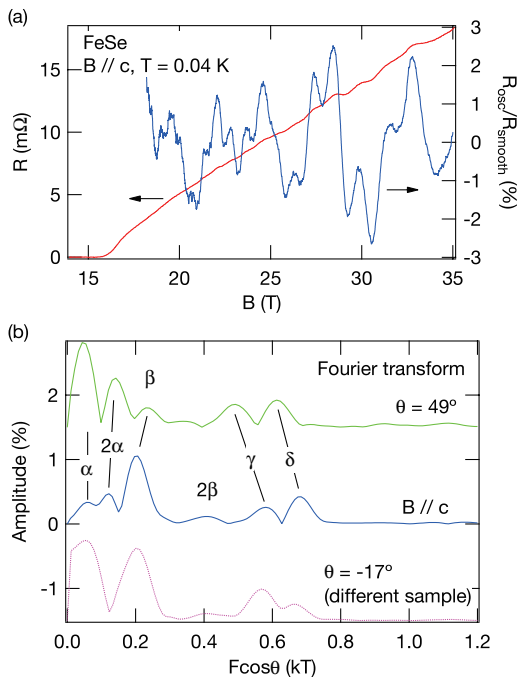


FIG. 1. (color online). (a) Resistance R and normalized oscillatory part $R_{osc}/R_{background}$ as a function of B . A fourth-order polynomial was fitted to the former above $B = 18$ T and was subtracted from it to obtain R_{osc} . (b) Fourier transforms of SdH oscillations in inverse field vs. $F \cos \theta$. Spectra for $\theta = 0$ and 49° were taken for sample 2, for -17° for sample 3. $T = 0.04$ K.

TABLE I. Experimental SdH frequencies, effective masses, orbit areas A , Fermi momenta and effective Fermi energies in FeSe for $B \parallel c$. The values were averaged over the four samples except for the α branch, for which the values are based on the second-harmonic data of sample 2. m_e is the free electron mass.

Branch	F (kT)	m^*/m_e	A (%BZ)	k_F (\AA^{-1})	E_F (meV)
α	0.06	1.9(2)	0.20	0.043	3.6
β	0.20	4.3(1)	0.69	0.078	5.4
γ	0.57	7.2(2)	2.0	0.13	9.1
δ	0.68	4.2(2)	2.3	0.14	18

III. RESULTS AND DISCUSSION

Figure 1(a) shows the resistance at $T = 0.04$ K in sample 2 as a function of B applied parallel to the c axis. After subtracting a smoothly varying background, we see clear SdH oscillations. Figure 1(b) shows Fourier transforms of the oscillations vs. $F \cos \theta$ for three field directions. The upper two spectra were obtained for sample 2, while the bottom one for sample 3. We find six frequency branches, α , 2α , β , 2β , γ , and δ . They are all small, and the corresponding orbits cover only 0.2–2.3% of the Brillouin zone [Table I and Fig. 3(b)]. Figure 2 shows the angle dependences of the SdH frequencies for samples 2 and 3. Note that the vertical axis is $F \cos \theta$. The two samples

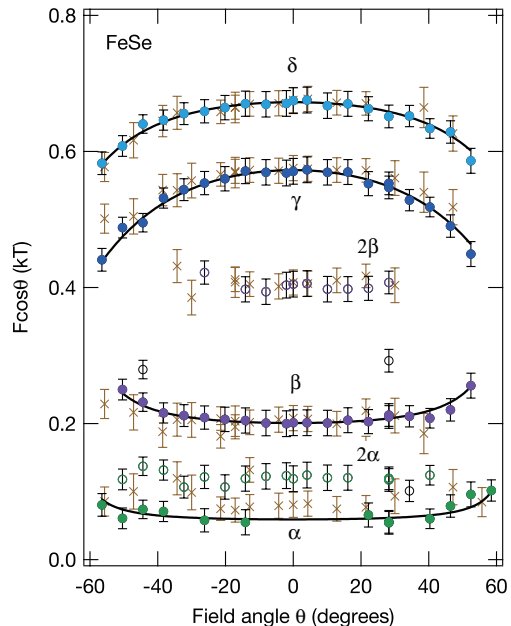


FIG. 2. (color online). Angle dependences of the SdH frequencies. The vertical axis is $F \cos \theta$. The circles and crosses are data for sample 2 ($T = 0.4$ K) and 3 ($T = 0.04$ K), respectively. For the former, different frequency branches are indicated by different colors, and harmonics are indicated by hollow marks. The solid curves are hyperboloidal- and ellipsoidal-surface fits to α and β , and γ and δ in sample 2, respectively (see Appendix B).

show consistent angle dependences. Although the data for sample 2 were those at $T = 0.4$ K because the angular variation was investigated more thoroughly in the ^3He refrigerator, no new frequency was found in additional measurements on this sample at $T = 0.04$ K. Within experimental accuracy, $F_{2\alpha} = 2F_\alpha$, and $F_{2\beta} = 2F_\beta$, indicating that the 2α and 2β frequencies are the second harmonics (we have also confirmed that $m_{2\beta}^* = 2m_\beta^*$ for $B \parallel c$ in sample 2). We have determined effective masses m^* for $B \parallel c$ from the temperature dependences of the oscillation amplitudes as tabulated in Table I. Mean free paths l can be estimated only roughly because of the limited range of inverse field. We find $l \sim 30$ and 80 nm for the β and δ orbits in sample 2, respectively.

We first consider the issue of the BCS-BEC crossover. An effective Fermi energy E_F can be estimated from experimental values of F and m^* using the following formulae: $E_F = \hbar^2 k_F^2 / (2m^*)$, $A = \pi k_F^2$, and $F = \hbar A / (2\pi e)$, where A is the orbit area in the k space and we have assumed circular orbits. The estimated Fermi energies are very small (Table I). Hence the ratio $k_B T_c / E_F$ is large, ranging between 0.04 (δ) and 0.22 (α). The proximity to the crossover may also be assessed by the parameter $(\xi k_F)^{-1}$ corresponding to $\sim \Delta / E_F$.^{18,19} Using $\xi = 5.7$ nm (see Appendix A for the upper critical field and coherence length) and the estimated k_F values (Table I), $(\xi k_F)^{-1} = 0.13$ (δ) and 0.41 (α). Since the BCS theory

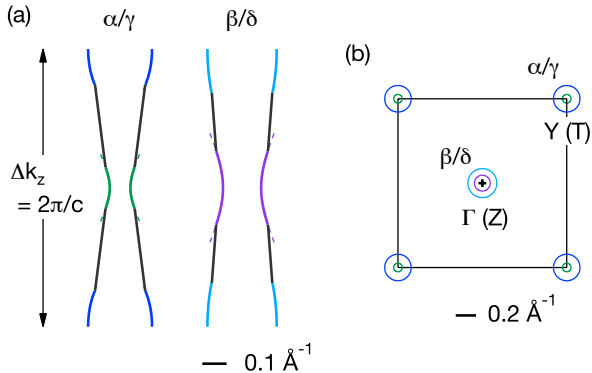


FIG. 3. (color online). Experimental Fermi surface cross-sections containing the k_z direction (a) and perpendicular to it (b). The in-plane anisotropy is ignored, and (b) is based on the second scenario (see text). The color coding is the same as that in Fig. 2 to show from which frequency branch each part of the cylinders is determined. The black lines in (a) indicate connecting regions between hyperboloidal and ellipsoidal ones.

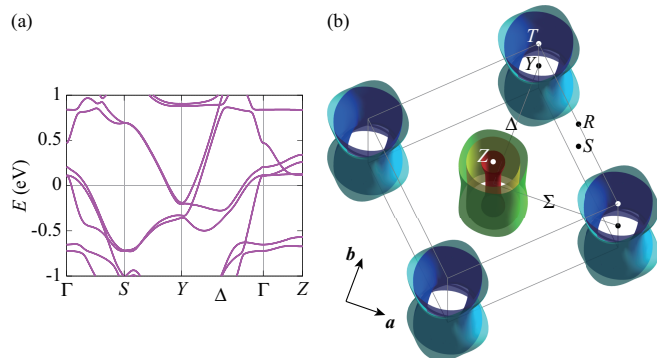


FIG. 4. (color online). Calculated band structure (a) and Fermi surface (b) of FeSe in the orthorhombic structure. The Γ point is the center of the Brillouin zone. The points Y, T, S, and R correspond to M, A, X, and R of the tetragonal Brillouin zone, respectively.

is based on the relation that $k_B T_c \sim \Delta \ll E_F$, these estimates suggest that the superconductivity in FeSe might not fully be understood within the BCS framework. Thus it seems worth looking for possible manifestations of the BCS-BEC crossover in FeSe, though they may substantially differ from those expected for single-band superconductors.

We now switch to the Fermi surface. The angular dependences in Fig. 2 indicate that the α and β frequencies are from minimal cross-sections, while γ and δ are from maximal ones. The former can be described by hyperboloidal surfaces while the latter by ellipsoidal surfaces as indicated by the solid curves in Fig. 2 (see Appendix B for details of the fits).

Based on these fits, we model the observed FS cylinders as shown in Fig. 3. We attribute α and γ to one cylin-

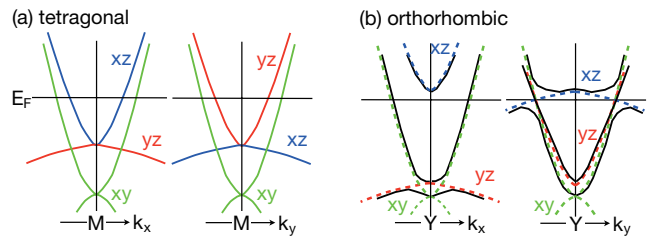


FIG. 5. (color online). Schematic of band reconstruction due to the orbital order. $k_x \parallel a$ and $k_y \parallel b$. (a) Band structure near the M points in the tetragonal phase. The two M points along k_x and k_y are equivalent except that the d_{xz} and d_{yz} orbital characters are inverted. (b) Band structure near the Y points in the orthorhombic phase. Because of the orbital order, the d_{xz} band is shifted up, while d_{yz} down as indicated by the broken lines. Since the bands anticross, they are eventually reconstructed as indicated by the solid lines, resulting in a single electron cylinder. (Note that, because of the choice $a < b$ in the orthorhombic phase, the shifts of the d_{xz} and d_{yz} bands are reversed in comparison to some previous works.^{5-8,17})

der and β and δ to another. This is the only reasonable combination: if β and γ were paired, extra minimum and maximum cross-sections would occur. Each cylinder has hyperboloidal, ellipsoidal, and connecting regions. We assume that the range of k_z for both hyperboloidal and ellipsoidal regions is restricted by that covered by orbits for $\theta = 55^\circ$. For larger $|\theta|$, orbits enter the cone-shaped connecting region outside this k_z range. The α/γ cylinder contains 0.0093 carriers/Fe and the β/δ 0.015 carriers/Fe. We can also estimate contributions of the observed FS cylinders to the Sommerfeld coefficient. Using the average of the effective masses for the minimum and maximum orbits for each cylinder with a two-dimensional approximation, we obtain 3.2 and 3.0 mJ/molK² for the α/γ and β/δ cylinders, respectively. Since the effective masses for the α and γ orbits differ considerably, the former may not be very accurate, and, if the large effective mass is restricted to the swollen region of the cylinder near the γ orbit, it may be an overestimate.

For the sake of comparison, we have performed band-structure calculations for the orthorhombic structure using the WIEN2K code²⁰ as shown in Fig. 4. The used lattice parameters are $a = 5.3078 \text{ \AA}$, $b = 5.3342 \text{ \AA}$, $c = 5.486 \text{ \AA}$,²¹ and $z_{\text{Se}} = 0.266689$.¹⁶ The calculated FS consists of two electron cylinders at the Y point of the Brillouin zone and three hole cylinders at the Γ point, similar to the iron-pnictide parent compounds. The calculated carrier density and Sommerfeld coefficient are $n_e = n_h = 0.17$ carriers/Fe and $\gamma_{\text{band}} = 4.6 \text{ mJ/mol K}^2$.

The question now is: are the two observed cylinders electrons or holes? Quantum oscillation measurements on the iron-pnictide parent compounds so far indicate that electron surfaces are generally easier to observe.²²⁻²⁶ It is thus tempting to assign the observed cylinders to the two calculated electron ones. However, considerations on the Sommerfeld coefficient are unfavorable to this sce-

nario. A previous specific-heat measurement on a single crystal of $\text{FeSe}_{0.963}$ in magnetic fields up to 9 T reported a Sommerfeld coefficient of $5.73 \pm 0.13 \text{ mJ/molK}^2$.²⁷ A recent measurement on vapor-grown FeSe at $B = 14 \text{ T}$ has found a similar value ($\sim 5.9 \text{ mJ/molK}^2$).²⁸ On the other hand, the sum of the above estimated coefficients for the observed cylinders is already 6.2 mJ/molK^2 . Further, at least one unobserved hole cylinder would have to exist in this scenario to satisfy the carrier compensation, and effective masses for the hole cylinder would most likely be no smaller than those for the electron ones (otherwise oscillations from the hole cylinder would have been detected). Hence the total would become still larger and be difficult to reconcile with the specific-heat data.

The above considerations lead us to assume that we have observed the whole Fermi surface consisting of an electron and a hole cylinder. We may assign the α/γ cylinder to electrons ($n_e = 0.0093$ carriers/Fe) and β/δ to holes ($n_h = 0.015$ carriers/Fe). Then, the small carrier imbalance is consistent with the Fe-deficient composition within error. As shown below, this second scenario means radical changes to the calculated band structure, but it can be reconciled with reported ARPES data.

We first consider the holes. Inspection of the calculated band structure along the ΓZ line [Fig. 4(a)] suggests that, because of the k_z dispersion of bands, it is difficult to have a single hole cylinder at Γ by simple constant band-energy shifts. On the other hand, ARPES measurements on FeSe indicate that only one hole band crosses the Fermi level at low temperatures to form a single hole sheet at ΓZ .^{6,7,9} Further, Ref. 9 suggests that the k_z dispersion of the hole band along the ΓZ line is $\sim 10 \text{ meV}$. This is consistent with our β/δ cylinder, for which the k_z dispersion can be estimated from the difference in the effective Fermi energies of the β and δ orbits to be 13 meV . Strictly, Ref. 9 claims that the hole band sinks below E_F in parts of the ΓZ line to form a closed pocket rather than a cylinder. However, this discrepancy could be attributed to surface effects such as surface band-bending.²⁹

We next turn to the electrons. In the tetragonal structure, if the spin-orbit coupling is neglected, the two electron bands responsible for the electron cylinders are degenerate by symmetry along the MX and AR lines, which correspond to the YS and TR lines of the orthorhombic Brillouin zone. Even if the spin-orbit coupling and tiny orthorhombic distortion ($|a - b|/(a + b) \sim 2 \times 10^{-3}$)¹⁶ are included in band-structure calculations, they remain quasi-degenerate along these lines and produce two electron cylinders as shown in Fig. 4. On the other hand, if we take the splitting of the d_{xz} and d_{yz} bands observed in ARPES measurements⁵⁻⁷ and anticrossing of bands into account, it is possible to have a single electron cylinder at the zone corner as illustrated in Fig. 5. Note however that this figure is very conceptual and that realistic models would have to include band renormalization and shifts, especially those of the d_{xy} band. Although the ARPES papers on FeSe do not state whether there is a

single electron cylinder or two, there is an ARPES study on NaFeAs which shows that, while two electron cylinders exist at the zone corner in the tetragonal phase, only one exists in the orthorhombic phase due to the electronic reconstruction at T_s .¹⁷

We now discuss a remarkable disparity between the calculated and observed carrier densities: $n_e = n_h = 0.17$ carriers/Fe vs. $n_e = 0.0093$ and $n_h = 0.015$ carriers/Fe. In iron-based superconductors, upward and downward shifts of electron and hole bands, respectively, relative to band structure calculations are often found, resulting in smaller Fermi surfaces.^{22-26,30} This FS shrinking has been attributed to electronic correlation effects, especially interband scattering.³¹⁻³³ For example, the Fermi surface of $\text{BaFe}_2(\text{As}_{1-x}\text{P}_x)_2$ shrinks as x is decreased from 1, while the mass enhancement, a measure of the correlations, and T_c increase.^{24,25} The carrier density at $x = 0.63$ is 0.05 carriers/Fe.²⁵ At $x = 0.41$, where $T_c \sim 25 \text{ K}$, the Fermi surface is roughly twice smaller than calculated.²⁴ However, the magnitude of the present shrinking is the largest ever observed. It is interesting to note that the observed carrier density is fairly comparable to that in the antiferromagnetic state of BaFe_2As_2 ($n_e = n_h = 0.006$ carriers/Fe),³⁴ where most of the paramagnetic FS has been destroyed by the reconstruction at the antiferromagnetic transition. There are some theoretical works on the electronic structure of FeSe where the dynamical mean-field theory (DMFT)^{33,35} or GW approximation³⁶ is used to treat the electronic correlations beyond the level of conventional band-structure calculations. They predict slightly modified Fermi surfaces compared to conventional calculations but can not explain our extremely small Fermi surface.

In conclusion, we have observed SdH oscillations in FeSe. Our analyses indicate that the Fermi surface in the orthorhombic state is very different from that expected from band-structure calculations, most likely consisting of one hole and one electron tiny cylinders. To elucidate how this radical deviation occurs is an urgent task, when effects of both the electronic correlations and the orbital order have to be considered. It will be very interesting to see how this anomalous Fermi surface evolves as T_c increases with pressure.

ACKNOWLEDGMENTS

This work has been supported by Japan-Germany Research Cooperative Program, KAKENHI from JSPS and Project No. 56393598 from DAAD, and the Topological Quantum Phenomena (No. 25103713) KAKENHI on Innovative Areas from MEXT of Japan. A portion of this work was performed at the NHMFL, supported by NSF Cooperative Agreement DMR-1157490, the State of Florida, and the US DoE. JSB acknowledges support from NSF-DMR 1309146.

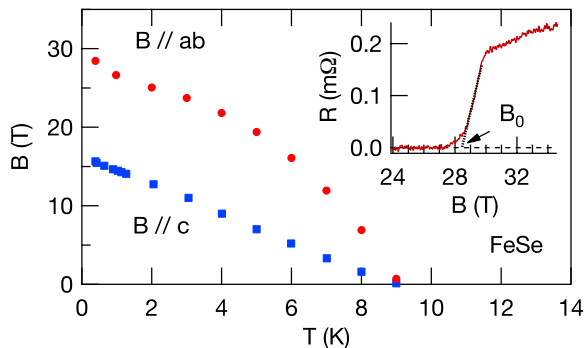


FIG. 6. Characteristic field B_0 in FeSe sample 2 as a function of temperature T . Inset: Resistance R as a function of field B applied parallel to the ab plane at $T = 0.39$ K. The definition of B_0 is given.

Appendix A: Upper critical field B_{c2} and coherence length ξ

Figure 6 shows the temperature (T) dependences of the characteristic field B_0 determined from R vs. B curves as explained in the inset. We assume that $B_0 \sim B_{c2}$. We use this unconventional definition because $R(B)$ curves for $B \parallel c$ are concave in the field range just above the superconducting resistive drop [see Fig. 1(a)] and hence the usual 50 or 90% resistive criterion for B_{c2} is ambiguous.

For $B \parallel c$, B_0 increases approximately linearly with decreasing T . A similar nearly linear or even convex variation of c -axis B_{c2} has been reported for other iron-based superconductors and has been explained by multiband effects.^{37–41} For $B \parallel ab$, B_0 shows a tendency to saturation down to ~ 2 K, suggesting paramagnetic limiting, but shows an anomalous enhancement below. A similar low- T enhancement has been reported for Fe(Se, Te)^{42,43} and (Ba,K)Fe₂As₂.⁴⁰

The initial slopes are -1.6 and -6.9 T/K for $B \parallel c$ and ab , yielding coherence lengths ξ of 1.3 and 5.7 nm for the c and ab directions, respectively.

The mass anisotropy $m_{\parallel c}/m_{\parallel ab}$ is estimated to be 19, which is larger than 9.5 found in LiFeAs,⁴⁴ contrary to the expectation that FeSe is more three-dimensional.

Appendix B: ellipsoidal and hyperboloidal-surface fits

For an ellipsoidal (+) or a hyperboloidal (–) Fermi surface $k_{ab}^2/(k_o^{ab})^2 \pm k_c^2/(k_o^c)^2 = 1$, where k_{ab} and k_c are the ab plane and c axis components of the k vector, respectively, the angle dependence of the frequency is given by $F(\theta) = F(0)[\cos^2 \theta \pm (k_o^{ab}/k_o^c)^2 \sin^2 \theta]^{-1/2}$. The fitting results shown in Fig. 2 are $(k_o^{ab} (\text{Å}^{-1}), k_o^c (\text{Å}^{-1}), \text{sign}) = (0.042, 0.086, -)$, $(0.078, 0.17, -)$, $(0.13, 0.24, +)$, and $(0.14, 0.37, +)$ for α, β, γ , and δ , respectively.

¹ Y. Kamihara, T. Watanabe, M. Hirano, and H. Hosono, *J. Am. Chem. Soc.* **130**, 3296 (2008).
² M. Rotter, M. Tegel, and D. Johrendt, *Phys. Rev. Lett.* **101**, 107006 (2008).
³ F.-C. Hsu, J.-Y. Luo, K.-W. Yeh, T.-K. Chen, T.-W. Huang, P. M. Wu, Y.-C. Lee, Y.-L. Huang, Y.-Y. Chu, D.-C. Yan, and M.-K. Wu, *Proc. Nat. Acad. Sci. U. S. A.* **105**, 14262 (2008).
⁴ K. Sasmal, B. Lv, B. Lorenz, A. M. Guloy, F. Chen, Y.-Y. Xue, and C.-W. Chu, *Phys. Rev. Lett.* **101**, 107007 (2008).
⁵ S. Tan, Y. Zhang, M. Xia, Z. Ye, F. Chen, X. Xie, R. Peng, D. Xu, H. X. Qin Fan, J. Jiang, T. Zhang, X. Lai, T. Xiang, J. Hu, B. Xie, and D. Feng, *Nat. Mater.* **12**, 634 (2013).
⁶ K. Nakayama, Y. Miyata, G. N. Phan, T. Sato, Y. Tanabe, T. Urata, K. Tanigaki, and T. Takahashi, arXiv:1404.0857 (2014).
⁷ T. Shimojima, Y. Suzuki, T. Sonobe, A. Nakamura, M. Sakano, J. Omachi, K. Yoshioka, M. Kuwata-Gonokami, K. Ono, H. Kumigashira, A. E. Böhmer, F. Hardy, T. Wolf, C. Meingast, H. v. Löhneysen, H. Ikeda, and K. Ishizaka, arXiv:1407.1418 (2014).
⁸ M. Yi, D. H. Lu, J.-H. Chu, J. G. Analytis, A. P. Sorini, A. F. Kemper, S.-K. Mo, R. G. Moore, M. Hashimoto, W. S. Lee, Z. Hussain, T. P. Devereaux, I. R. Fisher, and Z.-X. Shen, *PNAS* **108**, 6878 (2011).

⁹ Another ARPES study proposes a different interpretation for seemingly split bands at the zone corner: J. Maletz, V. B. Zabolotnyy, D. V. Evtushinsky, S. Thirupathiah, A. U. B. Wolter, L. Harnagea, A. N. Yaresko, A. N. Vasiliev, D. A. Chareev, A. E. Böhmer, F. Hardy, T. Wolf, C. Meingast, E. D. L. Rienks, B. Büchner, and S. V. Borisenko, *Phys. Rev. B* **89**, 220506 (2014).
¹⁰ Y. Mizuguchi, F. Tomioka, S. Tsuda, T. Yamaguchi, and Y. Takano, *Appl. Phys. Lett.* **93**, 152505 (2008).
¹¹ S. Medvedev, T. M. McQueen, I. A. Troyan, T. Palasyuk, M. I. Erements, R. J. Cava, S. Naghavi, F. Casper, V. Ksenofontov, G. Wortmann, and C. Felser, *Nat. Mater.* **8**, 630 (2009).
¹² W. Qing-Yan, L. Zhi, Z. Wen-Hao, Z. Zuo-Cheng, Z. Jin-Song, L. Wei, D. Hao, O. Yun-Bo, D. Peng, C. Kai, W. Jing, S. Can-Li, H. Ke, J. Jin-Feng, J. Shuai-Hua, W. Ya-Yu, W. Li-Li, C. Xi, M. Xu-Cun, and X. Qi-Kun, *Chin. Phys. Lett.* **29**, 037402 (2012).
¹³ S. Kasahara, T. Watashige, T. Hanaguri, Y. Kohsaka, T. Yamashita, Y. Shimoyama, Y. Mizukami, R. Endo, H. Ikeda, K. Aoyama, T. Terashima, S. Uji, T. Wolf, H. v. Löhneysen, T. Shibauchi, and Y. Matsuda, *Proc. Natl. Acad. Sci. USA* (to be published).
¹⁴ Y. Lubashevsky, E. Lahoud, K. Chashka, D. Podolsky, and A. Kanigel, *Nat. Phys.* **8**, 309 (2012).
¹⁵ K. Okazaki, Y. Ito, Y. Ota, Y. Kotani, T. Shimojima, T. Kiss, S. Watanabe, C.-T. Chen, S. Niitaka, T. Hanaguri, H. Takagi, A. Chainani, and S. Shin, *Sci. Rep.* **4**, 4109

- (2014).
- ¹⁶ A. E. Böhmer, F. Hardy, F. Eilers, D. Ernst, P. Adelman, P. Schweiss, T. Wolf, and C. Meingast, *Phys. Rev. B* **87**, 180505 (2013).
 - ¹⁷ Y. Zhang, C. He, Z. R. Ye, J. Jiang, F. Chen, M. Xu, Q. Q. Ge, B. P. Xie, J. Wei, M. Aeschlimann, X. Y. Cui, M. Shi, J. P. Hu, and D. L. Feng, *Phys. Rev. B* **85**, 085121 (2012).
 - ¹⁸ Q. Chen, J. Stajic, S. Tan, and K. Levin, *Phys. Rep.* **412**, 1 (2005).
 - ¹⁹ R. Sensarma, M. Randeria, and T.-L. Ho, *Phys. Rev. Lett.* **96**, 090403 (2006).
 - ²⁰ P. Blaha, K. Schwarz, G. K. H. Madsen, D. Kvasnicka, and J. Luitz, WIEN2K, edited by K. Schwarz (Technische Universität Wien, Austria, 2001).
 - ²¹ S. Margadonna, Y. Takabayashi, M. T. McDonald, K. Kasperkiewicz, Y. Mizuguchi, Y. Takano, A. N. Fitch, E. Suard, and K. Prassides, *Chem. Commun.*, 5607 (2008).
 - ²² A. I. Coldea, J. D. Fletcher, A. Carrington, J. G. Analytis, A. F. Bangura, J.-H. Chu, A. S. Erickson, I. R. Fisher, N. E. Hussey, and R. D. McDonald, *Phys. Rev. Lett.* **101**, 216402 (2008).
 - ²³ J. G. Analytis, C. M. J. Andrew, A. I. Coldea, A. McCollam, J.-H. Chu, R. D. McDonald, I. R. Fisher, and A. Carrington, *Phys. Rev. Lett.* **103**, 076401 (2009).
 - ²⁴ H. Shishido, A. F. Bangura, A. I. Coldea, S. Tonegawa, K. Hashimoto, S. Kasahara, P. M. C. Rourke, H. Ikeda, T. Terashima, R. Settai, Y. Ōnuki, D. Vignolles, C. Proust, B. Vignolle, A. McCollam, Y. Matsuda, T. Shibauchi, and A. Carrington, *Phys. Rev. Lett.* **104**, 057008 (2010).
 - ²⁵ J. G. Analytis, J.-H. Chu, R. D. McDonald, S. C. Riggs, and I. R. Fisher, *Phys. Rev. Lett.* **105**, 207004 (2010).
 - ²⁶ C. Putzke, A. I. Coldea, I. Guillamón, D. Vignolles, A. McCollam, D. LeBoeuf, M. D. Watson, I. I. Mazin, S. Kasahara, T. Terashima, T. Shibauchi, Y. Matsuda, and A. Carrington, *Phys. Rev. Lett.* **108**, 047002 (2012).
 - ²⁷ J.-Y. Lin, Y. S. Hsieh, D. A. Chareev, A. N. Vasiliev, Y. Parsons, and H. D. Yang, *Phys. Rev. B* **84**, 220507 (2011).
 - ²⁸ F. Hardy, Unpublished.
 - ²⁹ J. G. Analytis, J.-H. Chu, Y. Chen, F. Corredor, R. D. McDonald, Z. X. Shen, and I. R. Fisher, *Phys. Rev. B* **81**, 205407 (2010).
 - ³⁰ M. Yi, D. H. Lu, J. G. Analytis, J.-H. Chu, S.-K. Mo, R.-H. He, R. G. Moore, X. J. Zhou, G. F. Chen, J. L. Luo, N. L. Wang, Z. Hussain, D. J. Singh, I. R. Fisher, and Z.-X. Shen, *Phys. Rev. B* **80**, 024515 (2009).
 - ³¹ H. Zhai, F. Wang, and D.-H. Lee, *Phys. Rev. B* **80**, 064517 (2009).
 - ³² L. Ortenzi, E. Cappelluti, L. Benfatto, and L. Pietronero, *Phys. Rev. Lett.* **103**, 046404 (2009).
 - ³³ M. Aichhorn, S. Biermann, T. Miyake, A. Georges, and M. Imada, *Phys. Rev. B* **82**, 064504 (2010).
 - ³⁴ T. Terashima, N. Kurita, M. Tomita, K. Kihou, C. H. Lee, Y. Tomioka, T. Ito, A. Iyo, H. Eisaki, T. Liang, M. Nakajima, S. Ishida, S. Uchida, H. Harima, and S. Uji, *Phys. Rev. Lett.* **107**, 176402 (2011).
 - ³⁵ S. Mandal, R. E. Cohen, and K. Haule, *Phys. Rev. B* **89**, 220502 (2014).
 - ³⁶ J. M. Tomczak, M. van Schilfgaarde, and G. Kotliar, *Phys. Rev. Lett.* **109**, 237010 (2012).
 - ³⁷ F. Hunte, J. Jaroszynski, A. Gurevich, D. C. Larbalestier, R. Jin, A. S. Sefat, M. A. McGuire, B. C. Sales, D. K. Christen, and D. Mandrus, *Nature* **453**, 903 (2008).
 - ³⁸ H. Q. Yuan, J. Singleton, F. F. Balakirev, S. A. Baily, G. F. Chen, J. L. Luo, and N. L. Wang, *Nature* **457**, 565 (2009).
 - ³⁹ A. Gurevich, *Rep. Prog. Phys.* **74**, 124501 (2011).
 - ⁴⁰ T. Terashima, K. Kihou, M. Tomita, S. Tsuchiya, N. Kikugawa, S. Ishida, C. H. Lee, A. Iyo, H. Eisaki, and S. Uji, *Phys. Rev. B* **87**, 184513 (2013).
 - ⁴¹ D. A. Zocco, K. Grube, F. Eilers, T. Wolf, and H. v. Löhneysen, *Phys. Rev. Lett.* **111**, 057007 (2013).
 - ⁴² D. Braithwaite, G. Lapertot, W. Knafo, and I. Sheikin, *J. Phys. Soc. Jpn.* **79**, 053703 (2010).
 - ⁴³ C. Tarantini, A. Gurevich, J. Jaroszynski, F. Balakirev, E. Bellingeri, I. Pallecchi, C. Ferdeghini, B. Shen, H. H. Wen, and D. C. Larbalestier, *Phys. Rev. B* **84**, 184522 (2011).
 - ⁴⁴ N. Kurita, K. Kitagawa, K. Matsubayashi, A. Kismarhardja, E.-S. Choi, J. S. Brooks, Y. Uwatoko, S. Uji, and T. Terashima, *J. Phys. Soc. Jpn.* **80**, 013706 (2011).